Journal of Healthcare and Biomedical Science, Vol. 4 No. 2 (2026) https://doi.org/10.31098/jhbs.v4i2.4402

Check for updates

Research Paper

A Data-Centric Approach to HEK Cell Microscopic Image Segmentation using Multi-Scaling U-Net

Syiham Fakhrulradzi Abdul Aziz[1*], Ahmad Syahrin Idris[1], Siti Fauziah Toha[2], Izyan Mohd Idris[3], Muhammad Fauzi Daud[4], Azam Ahmad Bakir[5], Low Siow Yong[6]

[1] University of Southampton Malaysia, Malaysia

[2] International Islamic University Malaysia, Malaysia

[3] Institute for Medical Research (IMR); National Institutes of Health (NIH); Ministry of Health Malaysia, Malaysia

[4] Universiti Kuala Lumpur (UniKL), Malaysia

[5] Universiti Teknologi Malaysia, Malaysia

[6] University of Southampton Malaysia, Malaysia

Received : January 28, 2026	Revised : March 11, 2026	Accepted : June 14, 2026	Online : June 30, 2026

Abstract

Accurate and reproducible cell culture monitoring is important in biomedical research and regenerative medicine, yet manual assessment of cell confluency and morphology remains subjective and prone to inter-observer variability. Although deep learning approaches have been widely applied to cell segmentation, their systematic application to Human Embryonic Kidney (HEK) cells using data-centric methodologies remains underexplored. This study addresses this gap by implementing a Multi-Scaling U-Net (MSUNet) architecture combined with a data-centric workflow that emphasizes improving data quality through Contrast Limited Adaptive Histogram Equalization (CLAHE) preprocessing, Total Variation Denoising (TVD), and iterative expert-guided annotation refinement. The scope of analysis was limited to HEK293T cell images captured at 10x magnification using phase-contrast microscopy. The optimized model achieved an Intersection over Union (IoU) of 0.8980 after applying the data-centric approach, representing a 15.1% relative improvement over the baseline model trained without preprocessing or annotation refinement. These findings provide empirical evidence that systematic data quality improvement constitutes a key contributing factor to segmentation performance, offering a reproducible methodology for automated cell confluency measurement in resource-constrained laboratory settings.

Keywords *HEK293T Cells, Data-Centric AI, Biomedical Image Segmentation, Phase-Contrast Microscopy, Cell Confluency*

INTRODUCTION

Human Embryonic Kidney (HEK) cells and their variants represent one of the most widely utilized mammalian cell lines in modern biotechnology since their establishment in 1973 (Thomas & Smart, 2005). These cells serve central roles in recombinant protein production, viral vector manufacturing for gene therapy, and vaccine development, including recent applications in COVID-19 vaccine production (Seidel et al., 2023). The HEK293T variant, which incorporates the SV40 Large T-antigen to facilitate transfection, is particularly valued for high-yield protein expression and viral packaging applications.

In vitro cell culture of HEK cells is essential for both research and bio-manufacturing applications. Unlike immortalized cancer cell lines that can be readily biopsied, HEK cells cannot be repeatedly harvested from their original embryonic source due to ethical constraints. Moreover, industrial scale biotherapeutic production requires billions of cells under controlled, reproducible

Corresponding author's: msaa1e24@soton.ac.uk

conditions, quantities impossible to obtain from primary tissue sources. Established cell lines like HEK293T provide standardized biological material with consistent characteristics across passages, enabling reproducible experimental results and regulatory compliance in biomanufacturing. However, maintaining optimal culture conditions throughout the growth cycle requires careful monitoring, particularly of cell confluency.

Cell culture monitoring is central to biomedical research and biomanufacturing, yet it remains predominantly manual, labor-intensive, and susceptible to inter-observer variability. Traditional methods, such as hemocytometer counting and visual microscopy inspection, can vary by up to 20% between operators (Liu et al., 2024), creating challenges for reproducibility in research and quality control in biotherapeutic production (Singh et al., 2025). Despite their widespread use in biomanufacturing, dedicated automated segmentation systems for HEK cells remain limited in the literature: a comprehensive survey of deep learning applications in microscopy image analysis (Liu et al., 2021) covers segmentation across blood cells, cancer cells, and corneal endothelial cells, but does not include any studies specifically targeting HEK cell segmentation, reflecting the limited presence of HEK-specific work in the broader literature. HEK cells present particular challenges including semi-transparent appearance under phase-contrast microscopy and irregular, elongated morphologies that generic segmentation models may not optimally capture.

The emergence of deep learning, particularly convolutional neural networks (CNNs), has opened new possibilities for automated cell image analysis. However, the dominant research paradigm has been model-centric, focusing on architectural innovations while treating datasets as fixed constraints (Bhatt et al., 2024). Recent advances in data-centric artificial intelligence (DCAI) challenge this assumption, demonstrating that systematic data quality improvements can yield performance gains equal to or exceeding architectural modifications (Zha et al., 2025). Data preprocessing techniques such as Contrast Limited Adaptive Histogram Equalization (CLAHE) have shown considerable impact, improving segmentation accuracy by up to 4.5% in kidney segmentation tasks (Buriboev et al., 2024) and markedly improving Dice similarity coefficients in medical image analysis (Yoshimi et al., 2024). Despite these promising results, the systematic application of data-centric principles to cell segmentation remains underexplored, with most studies continuing to emphasize model architecture optimization over data quality considerations.

Current research gaps can be identified across three dimensions. First, while U-Net architecture has been extensively applied to various cell types including stem cells, cancer cells, and blood cells, HEK cell segmentation is notably absent from coverage in comprehensive deep learning microscopy surveys (Liu et al., 2021), despite their major importance in biomanufacturing. The unique morphological characteristics of HEK cells require targeted solutions that generic segmentation models may not optimally provide. Second, although data-centric AI principles have gained theoretical recognition through workshops at major conferences (NeurIPS, ICML, ICLR) and MIT's DCAI initiative, their practical application to cell segmentation tasks remains limited (Whang et al., 2023). Third, comparative evaluations quantifying the specific contribution of data quality improvements versus architectural choices are rarely reported in cell segmentation literature, making it difficult to establish evidence-based best practices for resource allocation in developing automated monitoring systems.

This study addresses these gaps through a data-centric approach to HEK cell segmentation. The research implements a Multi-Scaling U-Net architecture (Shamhan et al., 2023) optimized for capturing multi-scale features necessary for accurate boundary detection in cells with variable sizes and irregular morphologies. More importantly, this work systematically applies data-centric methodologies, including CLAHE preprocessing for contrast enhancement, Total Variation Denoising (TVD) for noise reduction while preserving edges, and expert-guided iterative

refinement of ground truth annotations, and documents segmentation performance before and after applying these techniques.

This work is expected to make three contributions, contingent on the results obtained: (1) empirical evaluation of data-centric approaches for HEK cell segmentation on a single controlled dataset, (2) quantitative comparison of model performance before and after data quality interventions (targeting IoU improvement from a baseline of 0.781), and (3) a reproducible methodology combining multi-scale architecture with data-centric preprocessing adaptable to other cell types.

This research aims to develop and validate a data-centric deep learning approach for automated HEK cell segmentation to improve cell culture monitoring accuracy and efficiency. Specifically, the objectives are: (1) to implement a Multi-Scaling U-Net architecture for HEK cell segmentation, capable of handling variable cell sizes and irregular morphologies characteristic of this cell line; (2) to apply data-centric preprocessing techniques, including CLAHE and TVD, to enhance image quality, and to incorporate feedback from cell culture experts to refine ground-truth annotations; and (3) to benchmark the developed approach against a baseline model, documenting performance improvements achieved through data-centric methodologies.

The remainder of this paper is organized as follows: Section 2 presents a detailed literature review covering challenges in cell culture monitoring, deep learning architectures for biomedical image segmentation, and data-centric AI principles. Section 3 describes the methodology. Section 4 presents experimental results. Section 5 discusses implications, limitations, and future directions. Section 6 concludes the paper.

LITERATURE REVIEW

HEK Cell Segmentation: Challenges and Gaps

HEK293T cells are among the most widely used mammalian cell lines in biomanufacturing, yet automated segmentation systems designed specifically for this cell type remain scarce. Manual monitoring through hemocytometer counting and visual microscopy inspection is the prevailing approach, but it is fundamentally limited by inter-observer variability of up to 20% between operators (Liu et al., 2024). This variability undermines reproducibility in research and poses quality-control risks in biotherapeutic production (Singh et al., 2025), particularly because HEK cells cannot be re-harvested from their original embryonic source and must therefore be maintained under consistent culture conditions across passages (Thomas & Smart, 2005).

The segmentation of HEK cells presents distinct challenges that generic models are not optimized to address. Under phase-contrast microscopy, HEK cells exhibit semi-transparent appearances and irregular, elongated morphologies that make boundary delineation difficult even for experienced human annotators (Seidel et al., 2023). In high-confluency conditions, cells form dense clusters with indistinct intercell boundaries, further complicating pixel-level classification. A comprehensive survey of deep learning applications in microscopy image analysis (Liu et al., 2021) covers blood cells, cancer cells, corneal endothelial cells, and nucleus segmentation, but does not include any studies targeting HEK cell segmentation, consistent with its limited presence in broader literature. This gap is particularly notable given HEK cells' extensive use in producing recombinant proteins and viral vectors for gene therapy, applications where precise confluency measurement directly affects production yield and regulatory compliance.

Existing automated approaches for cell culture monitoring more broadly include threshold-based methods and traditional image processing pipelines. Conventional segmentation methods, such as thresholding and edge-based algorithms, produce imperfect contours and lack the generalization capacity needed to accommodate diverse imaging conditions and cell morphological variations (Chai et al., 2024). The combination of these limitations with the absence of HEK-specific

segmentation solutions motivates the development of a targeted deep learning approach grounded in systematic data quality improvement.

U-Net-Based Deep Learning for Biomedical Segmentation

Suitability of CNN Architectures for Cell Segmentation

The encoder-decoder U-Net architecture introduced by Ronneberger et al. (2015) remains the most widely adopted framework for biomedical image segmentation. Its key design feature, skip connections between encoder and decoder paths, allows the network to combine high-level semantic features with low-level spatial detail, enabling precise boundary localization even when trained on small, annotated datasets. This characteristic is directly relevant to HEK cell segmentation, where training data is limited by the cost of expert annotation and the ethical restrictions on data acquisition (Dhar et al., 2023).

The spatial inductive biases inherent in convolutional operations, translation invariance, and local receptive fields align naturally with cell boundary detection tasks, where relevant features are local and spatially consistent across the image. For datasets of fewer than 2,000 images, CNNs consistently outperform data-hungry alternatives such as Vision Transformers (Takahashi et al., 2024), making them the appropriate architectural choice for the HEK cell dataset used in this study.

Advances and Limitations of U-Net Variants

Several U-Net variants have further improved segmentation performance in biomedical contexts. CellSegUNet integrates attention mechanisms with UNet++ and Residual UNet architectures for cell nucleus segmentation, achieving superior boundary delineation through serial and parallel feature connections (Metlek, 2024). Enhanced U-Net architectures with modified encoder branches have also demonstrated consistent performance gains over vanilla baselines (Long, 2020). Despite these advances, a key limitation shared across U-Net variants is the loss of fine-grained spatial information through max-pooling operations, which can reduce boundary precision in densely packed cell regions (Riandini et al., 2023).

Alternatives such as Vision Transformers require millions of training samples to achieve competitive performance (Han et al., 2023) and underperform CNNs on datasets with fewer than 10,000 images (Takahashi et al., 2024), conditions directly applicable to this study. Recurrent Neural Networks offer advantages for time-lapse cell tracking (Chu et al., 2020; Spilger et al., 2020) but provide no benefit for static single-frame segmentation. Generative Adversarial Networks can augment limited datasets through synthetic image generation (Baniukiewicz et al., 2019) but do not directly perform segmentation. Graph Neural Networks model cell-cell interactions effectively (Ben-Haim & Raviv, 2022) but introduce unnecessary complexity for pixel-wise boundary detection in static images.

The Multi-Scaling U-Net (MSUNet) adopted in this study (Shamhan et al., 2023) extends the base U-Net by processing each encoder block through dual parallel convolutional streams with different kernel sizes (3×3 and 5×5), enabling simultaneous capture of fine-grained and contextual features. This multi-scale design is particularly well-suited to HEK cell segmentation, where cells vary considerably in apparent size depending on confluency level and imaging conditions.

Data-Centric AI: From Theory to Practice in Cell Segmentation

The Shift from Model-Centric to Data-Centric Thinking

The dominant paradigm in deep learning research has historically been model-centric: architectural innovations and hyperparameter tuning are pursued while training datasets are treated as fixed inputs (Bhatt et al., 2024). Data-centric AI (DCAI), as formalized through the MIT DCAI initiative and workshops at NeurIPS, ICML, and ICLR, challenges this assumption by repositioning dataset quality as the primary lever for performance improvement (Zha et al., 2025). The core insight is that in practical applications, especially medical imaging, data quality issues, including noise, inconsistent annotations, class imbalance, and domain shift, frequently constitute the binding constraint on model performance, not architectural complexity (Whang et al., 2023).

This reframing is particularly relevant for HEK cell segmentation, where architectural choices are constrained by dataset size and computational resources, but data quality is tractable through targeted preprocessing and expert annotation refinement. Empirical studies have confirmed that systematic data quality improvement can yield performance gains comparable to or exceeding those from architectural innovations (Bhatt et al., 2024), while avoiding the additional computational demands of larger or more complex models.

Preprocessing as a Data Quality Intervention

Preprocessing techniques directly address image quality issues arising from the imaging process itself. Contrast Limited Adaptive Histogram Equalization (CLAHE), introduced by Zuiderveld (1994), enhances local contrast by equalizing histograms within spatially limited tiles and applying contrast clipping to prevent over-amplification. For phase-contrast microscopy images, where HEK cells appear semi-transparent against a similarly-toned background, CLAHE makes subtle cell boundaries more distinguishable, reducing the ambiguity that causes segmentation failures at low confluency levels (Hayati et al., 2023; Musa et al., 2018). In kidney segmentation on the KiTS19 dataset, modified CLAHE reduced BRISQUE quality scores from 28.8 to 21.1 and improved CNN segmentation accuracy from 0.951 to 0.996 (Buriboev et al., 2024). Improved Dice similarity coefficients following CLAHE preprocessing have also been reported in temporomandibular joint segmentation on MRI (Yoshimi et al., 2024), demonstrating its generalizability across imaging modalities.

A well-known side-effect of CLAHE is the amplification of high-frequency image noise. Total Variation Denoising (TVD), introduced by Chambolle (2004), addresses this by minimizing total variation in the image while preserving edge structures. Applied after CLAHE, TVD suppresses background noise and imaging artifacts without blurring genuine cell boundaries, directly targeting the false-positive detection failure mode common in phase-contrast cell segmentation (Tang & Fang, 2016). The combination of CLAHE followed by TVD thus addresses two complementary data quality problems: insufficient contrast and excessive noise.

Annotation Quality as a Data-Centric Intervention

Beyond image preprocessing, ground truth annotation quality is a critical determinant of supervised segmentation performance. Label noise, errors, inconsistencies, or ambiguities in annotated masks propagate directly into model learning, introducing systematic biases that preprocessing alone cannot resolve (Luca et al., 2022). In medical image segmentation, annotation is typically performed by non-expert researchers whose labeling decisions may not align with biological ground truth, particularly at ambiguous boundaries such as the edges of dense HEK cell clusters (Dhar et al., 2023).

Expert-guided iterative annotation refinement, in which a domain specialist reviews and

corrects preliminary labels, directly reduces this label noise. This approach is consistent with data-centric AI principles that treat annotation quality as an engineering problem rather than a fixed input (Whang et al., 2023). The annotation refinement process in this study involved three structured review cycles with a cell culture specialist from IMR, targeting boundary accuracy and systematic misclassification correction, interventions expected to yield measurable improvements in segmentation performance independently of any architectural change.

Conceptual Framework and Study Positioning

The three pillars reviewed above converge on a clear conceptual framework for this study. HEK cell segmentation is an underaddressed problem, with imaging challenges and limited annotated data making data quality the dominant performance bottleneck. CNN-based U-Net architectures, specifically MSUNet with its multi-scale feature extraction, are well-matched to this problem, given dataset size constraints. Data-centric interventions (CLAHE, TVD, and expert annotation refinement) are expected to improve segmentation performance through two independent mechanisms: cleaner input features and more accurate training targets. By holding the model architecture constant across baseline and enhanced conditions, this study isolates the empirical contribution of data quality improvement, providing evidence that addresses the third gap identified in the literature: the lack of comparative evaluations quantifying data quality versus architectural contributions to segmentation performance.

RESEARCH METHOD

Experimental Setup

Segmentation Model Architecture

Multi-Scaling U-Net (MSUNet) from (Shamhan et al., 2023) is used as the segmentation model. Each encoder block processes the input feature map through two parallel convolutional streams with different kernel sizes (3 x 3 and 5 x 5), allowing the network to capture both fine details and broader contextual features. After dropout regularization, the outputs of these streams are concatenated and passed through a 1 x 1 convolution to fuse the multi-scale information into a unified representation.

The contracting path consists of four encoder blocks with progressively doubled feature channels (16, 32, 64, 128), separated by 2 × 2 max pooling for spatial down-sampling. The bottleneck layer has 256 channels and follows the same multi-scale design. The expansive path mirrors the encoder structure, using transposed convolutions for up-sampling. At each level, the upsampled feature maps are concatenated with the corresponding encoder features (skip connections) before passing through a multi-scale convolutional block. The final layer applies a 1 x 1 convolution with sigmoid activation to produce a binary mask indicating the predicted cell regions. Figure 1 illustrates the model architecture:

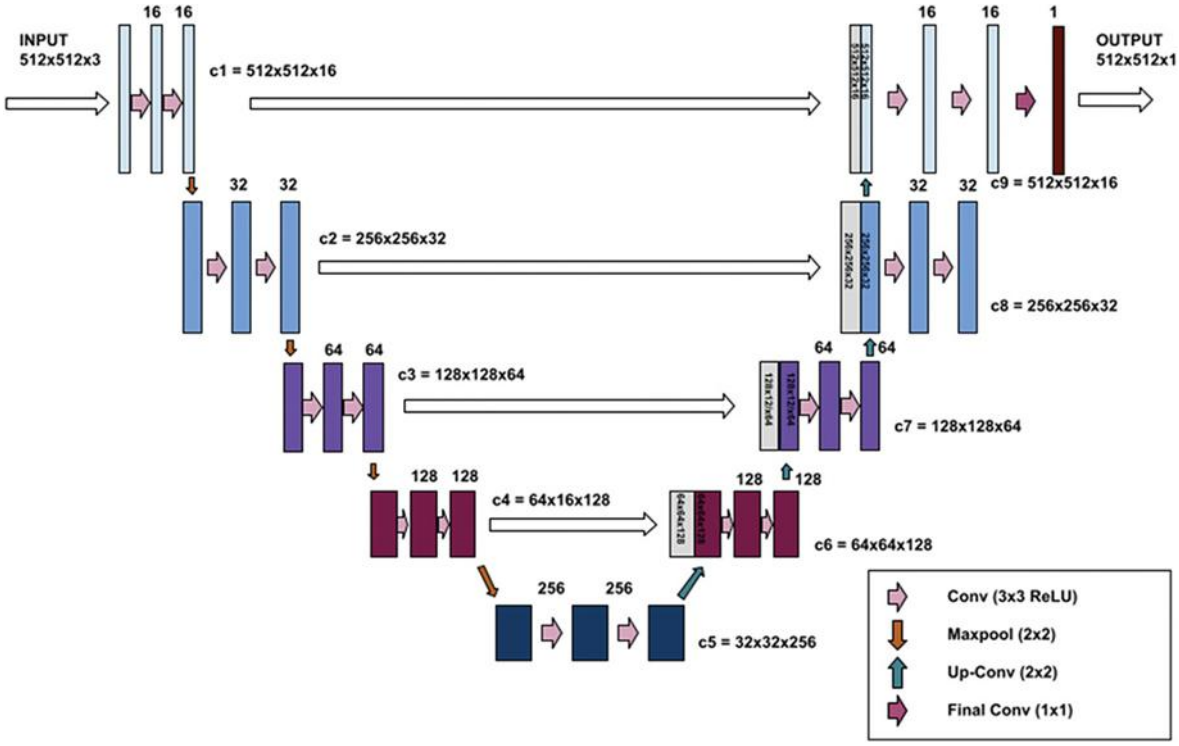

Figure 1. MSUNet Model Architecture (Shamhan et al., 2023)

Computer Hardware and Training Settings

All experiments were conducted using Tensorflow and the Keras API, with the segmentation_models library for specialized metrics and loss functions. The model was implemented in Python 3.10 and executed on a Windows 11 workstation. The hardware configuration included an NVIDIA GPU (CUDA-enabled) with 4 GB VRAM, 16 GB system RAM, and an Intel Core i7 processor. GPU acceleration was utilized to enable faster training and evaluation.

Data normalization was applied to all inputs, and masks were rescaled to binary values (0 and 1). To prevent data leakage, the 80%/20% train-test split was performed at the original image level before any patching. This ensures that all 256×256 patches derived from a given source image appear exclusively in either the training set or the test set, not both. The split was performed using train_test_split with a fixed random seed for reproducibility.

The Adam optimizer with a learning rate of 0.001 was employed. The model was trained with a batch size of 2 over 50 epochs. To address class imbalance and improve segmentation performance, a hybrid loss function was adopted, combining Dice Loss and Binary Focal Loss.

Evaluation Criteria

1. Confusion Matrix

The basis for most segmentation metrics lies in the confusion matrix, which consists of four key components: true positives (TP), false positives (FP), true negatives (TN), and false negatives (FN). These are summarized in Table 1:

Table 1. Confusion Matrix Elements

Terms	Descriptions	Remarks
True Positive (TP)	Correctly predicted cell pixels	Merit
True Negative (TN)	Correctly predicted background pixels	Merit
False Positive (FP)	Background pixels misclassified as cells	Demerit
False Negative (FN)	Cells pixels misclassified as background	Demerit

2. Pixel Accuracy

Pixel accuracy quantifies the proportion of correctly classified pixels over the total number of pixels:

$$Accuracy = \frac{TP + TN}{TP\ +\ TN + FP + FN} \tag{1}$$

3. Intersection-over-Union

IoU measures the overlap between predicted segmentation masks and the ground-truth masks:

$$IoU = \frac{TP}{TP\ +\ FP + FN} = \frac{R_{GT}\ \cap\ R_{PS}}{R_{GT}\ \cup\ R_{PS}} = \frac{labels\ \cap\ predictions}{labels\ \cup\ predictions} \tag{2}$$

4. Intersection-over-Union

$$Precision = \frac{TP}{TP\ +\ FP} \tag{3}$$

$$Recall = \frac{TP}{TP\ +\ FN} \tag{4}$$

5. Dice Coefficient (F1-Score)

$$F_{score} = \frac{2\ \times Precision\ \times Recall}{Precision\ +\ Recall} \tag{5}$$

Loss Function

In segmentation tasks, the choice of loss function plays an important role in guiding the model towards learning meaningful boundaries and overcoming class imbalance. Since HEK cell images typically contain a large proportion of background pixels compared to relatively small cell regions, conventional loss functions such as binary cross-entropy may lead to suboptimal performance. To address this, focal loss (FL) was used as a derivation of the cross-entropy loss function that would downweight easy examples and focus training on hard negatives, mitigating the impact of the dominant background pixels.

$$CE(p) = -y \log p - (1 - y) \log(1 - p) \tag{6}$$

$$CE(p) = -\log p \tag{7}$$

$$BCE(p) = -\alpha \log p \tag{8}$$

$$FL(p) = -\alpha(1 - \mathrm{p})^{\gamma} \log p \tag{9}$$

Where $y \in \{0,1\}$ are ground truth classes and $\mathrm{p} \in [0,1]$ are estimated true class probabilities

with class y = 1.

Another loss that was employed in this study is Dice Loss. It aims to minimize the mismatch between ground truth and predicted segmentation and optimize segmentation metrics such as the Dice coefficient and IoU.

$$Dice\ Coefficient = \frac{2|R_{GT} \cap R_{PS}|}{|R_{GT}| + |R_{PS}|} = \frac{2yp + 1}{y + p + 1} \quad (10)$$

$$DL(p) = 1 - \frac{2yp + 1}{y + p + 1} \quad (11)$$

Where R_{GT} is the ground truth region and R_PS is the predicted segmentation region. This hybrid approach has demonstrated marked improvements in biomedical tasks (Yeung et al., 2022, 2023; Zheng et al., 2022).

Data Acquisition and Annotation

This study utilized datasets consisting of HEK cells for growth. The HEK cells are HEK 293T, modified from the HEK lineage. The total collected images from the Institute of Medical Research (IMR) Malaysia amount to 1827 images, with dimensions of 2048 x 1536 pixels, using phase-contrast microscopy. Detailed information is shown in Table 2:

Table 2. Data Collection Details

Provider	Institute of Medical Research (IMR) Setia Alam Period: July 2025- Sep 2025
Cell Type	HEK Cell
Image Type	X10 magnification level
Modality	Phase-contrast microscopy
Image Size	2048 x 1536 pixels
Number of Images	1827

In the experiments, the HEK cells were allowed to grow and reach maximum confluency for up to 7 days, depending on the initial number of cells placed in the petri dish. The datasets show significant differences in terms of their features, particularly the shape of the cells, as they grow. HEK cells grow individually and have elongated shapes, as shown in Figure 2.

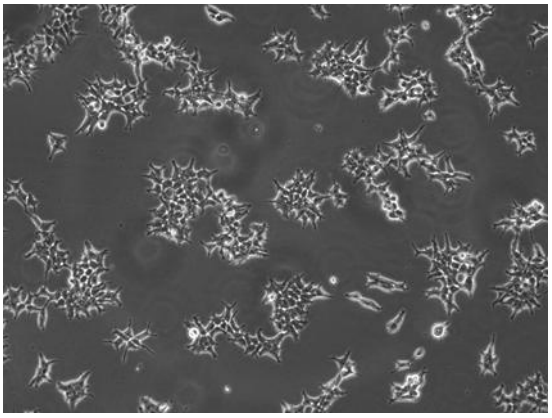

Figure 2. HEK Cell

X10 Magnification is set across all images because it provides a balance between capturing sufficient structural detail of individual cells and maintaining a wide enough field of view to analyze cell colonies and confluency trends. Thus, X10 was selected as an optimal trade-off for segmentation purposes. The setup information is listed in Table 3:

Table 3. EVOS M5000 Setup Information

Instrument	Parameter	Control Protocol
Evos M5000 Imaging System	Dimension	2048 x 1536
	Modality	Phase-Contrast
	Light	2.904
	Sharpness	Analog
	Color Channel	TRANS (grayscale)

From the full collection of 1,827 images, 40 images spanning the complete confluency range (approximately 20% to 95%) were selected for training. This number was determined by the hardware constraint of 4 GB VRAM, which limited the feasible batch size and total dataset volume; it is also consistent with small-dataset deep learning practices demonstrated in the original U-Net paper, which achieved strong segmentation performance with as few as 30 annotated images (Ronneberger et al., 2015). After patching and filtering, the 40 images yielded 1,920 representative 256×256 patches for training. The ground truth image has been annotated by labelling the cell region with pixel value '1' and the background as pixel value '0' as shown in Figure 3:

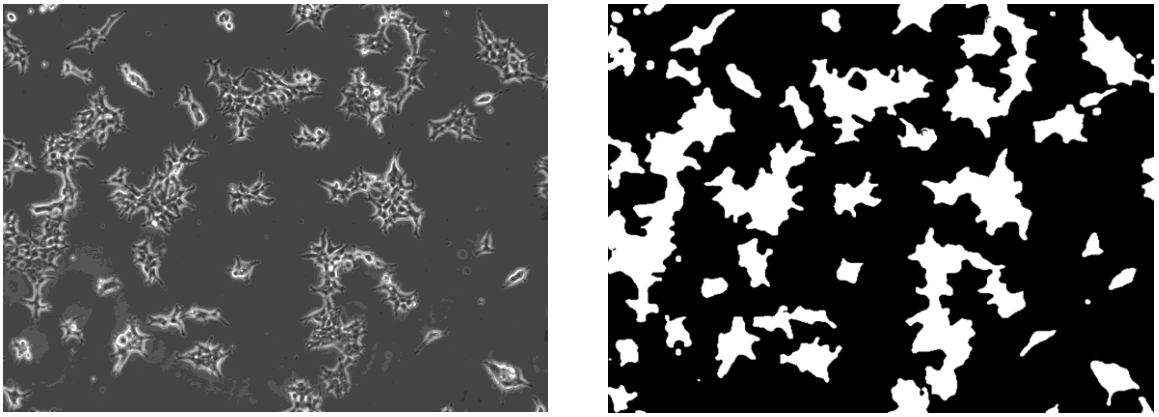

(a) Original Image (b) Ground Truth

Figure 3. Example of Inputs for Segmentation Model

Data Quality Assurance and Bias Control

Sampling Strategy and Selection Criteria

The selection of training images followed a stratified purposive sampling approach designed to ensure representation across the full range of cell culture growth stages. From the total collection of 1,827 HEK293T cell images, 40 images were systematically selected to span confluency levels from approximately 20% to 95%, capturing the complete spectrum of cell density conditions encountered in typical culture workflows. Images were selected at regular confluency intervals (approximately 15-20% increments) to provide a balanced representation of sparse, moderate, and dense cell populations. This sampling strategy was necessary to enable the model to learn features characteristic of cells at different growth stages while maintaining computational feasibility, given hardware constraints (4GB VRAM limitation).

Selection criteria included: (1) image sharpness and focus quality confirmed through manual inspection, (2) absence of obvious imaging artifacts such as debris or contamination, (3) diverse spatial distributions of cells within the field of view, and (4) representation of typical morphological variations observed in HEK cell cultures, including both individual cells and cell clusters. Images exhibiting poor focus, excessive debris, or atypical culture conditions were excluded from the training set to prevent the model from learning non-representative features.

Bias Control and Annotation Quality Assurance

Annotation bias represents a significant concern in supervised learning for biomedical image segmentation. Given the researcher's limited domain expertise in cell culture, these preliminary annotations were subject to systematic review by a culture specialist from the Institute of Medical Research (IMR) with experience in HEK cell culture and microscopy analysis.

The expert independently reviewed all 40 annotated images and provided detailed feedback on boundary accuracy, identification of ambiguous regions, and correction of systematic misclassifications. This iterative refinement approach ensured that ground truth labels reflected expert knowledge rather than inexperienced annotator interpretation. Ground truth annotations were initially prepared by the researcher and subsequently reviewed through a consensus-based process with cell culture specialists from the Institute for Medical Research (IMR), Malaysia. While no formal inter-annotator agreement metric was computed, the consensus review approach ensures that final annotations reflect collective expert judgement rather than a single annotator's interpretation.

Reproducibility

To enhance reproducibility, all training procedures employed fixed random seeds (seed=42) for data splitting and initialization. The train-test split allocation (80%/20%) was performed using scikit-learn's train_test_split function with stratification disabled due to the continuous nature of confluency levels. Model training utilized deterministic operations where possible, though complete reproducibility is limited by inherent stochasticity in GPU operations. It is also acknowledged that results are reported from a single training run; the absence of repeated experiments with statistical variance reporting is a limitation of this study, discussed further in Section 5.

Image Preprocessing for a Data-Centric Approach

Image Preprocessing for Inappropriate Imaging Quality

CLAHE was introduced by Zuiderveld (1994) and was chosen to correct the image color for better distinguished annotation and segmentation process. CLAHE is applied per tile to improve the visibility level of objects in foggy images by stretching the histogram, limiting the contrast, and performing bilinear interpolation at the edges to match the next tiles. Figure 4 illustrates the potential results before and after the application of CLAHE.

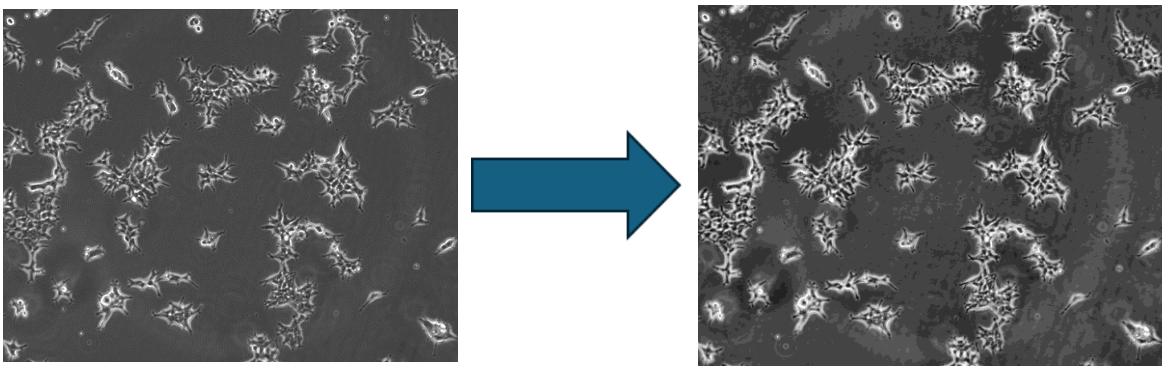

Figure 4. CLAHE Image Preprocessing

Total Variation Denoising (TVD)

One common side-effect of using the CLAHE technique is the introduction of noise into the image. TVD (Chambolle, 2004) effectively reduces noise while retaining the benefits of CLAHE in terms of improved visualization of object edges. Its regularization parameter of 0.1 was set for each trial.

Image Patching for High-Resolution Images

Each image has a resolution of 2048 x 1536 pixels based on data collection. For training, the images are deemed too large to be handled by the computational power available at the time. To avoid heavy loss of model training, the images were patched into several smaller input sizes, as portrayed in Figure 5, each of which can still represent the object features; thus, the optimal patch size is dependent on the datasets. The expected number of patches that will be generated can be calculated using the following equation:

$$Number\ of\ patches = \frac{Image\ Width}{Target\ Size} \times \frac{Image\ Height}{Target\ Size} \tag{12}$$

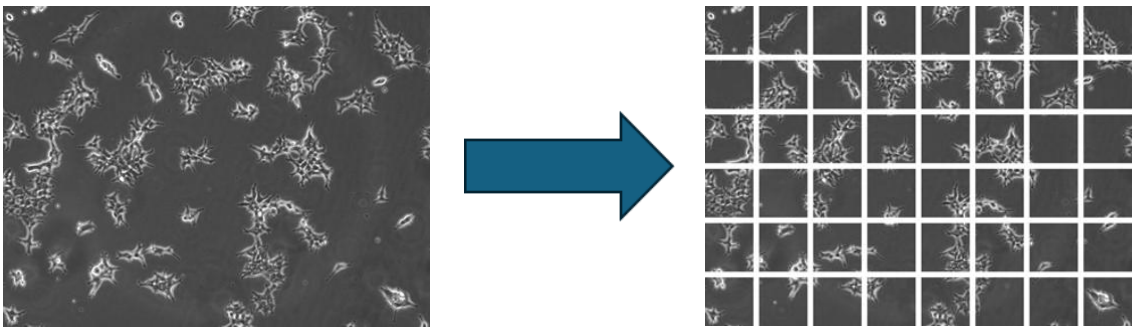

Figure 5. Image Patching

Filtering for Class Imbalance

In the context of this study, an imbalanced dataset can occur when training images contain either cells or background only. Therefore, it is crucial to employ precautions that help to balance the dataset. One such approach is filtering out non-representative patches that contain an excessive number of background pixels. Patches with no cell pixels occupied were removed, as shown in Figure 6:

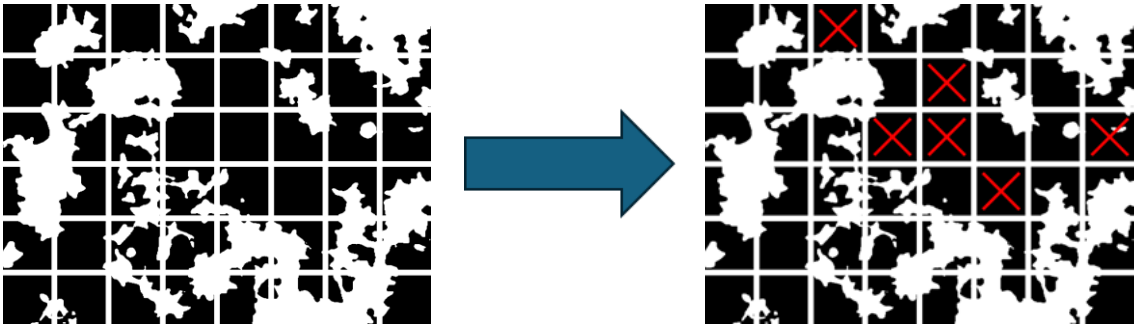

Figure 6. Patch Filtering

Patch-Based Segmentation Pipeline

The original images are 2048 x 1536 pixels in size, and the model is trained using the selected patch size during training. The original images will be patched first, and cells will be segmented by patches. After each segmented patch is completed, the patches are unpatched to obtain the original images with true class labels, as shown in Figure 7.

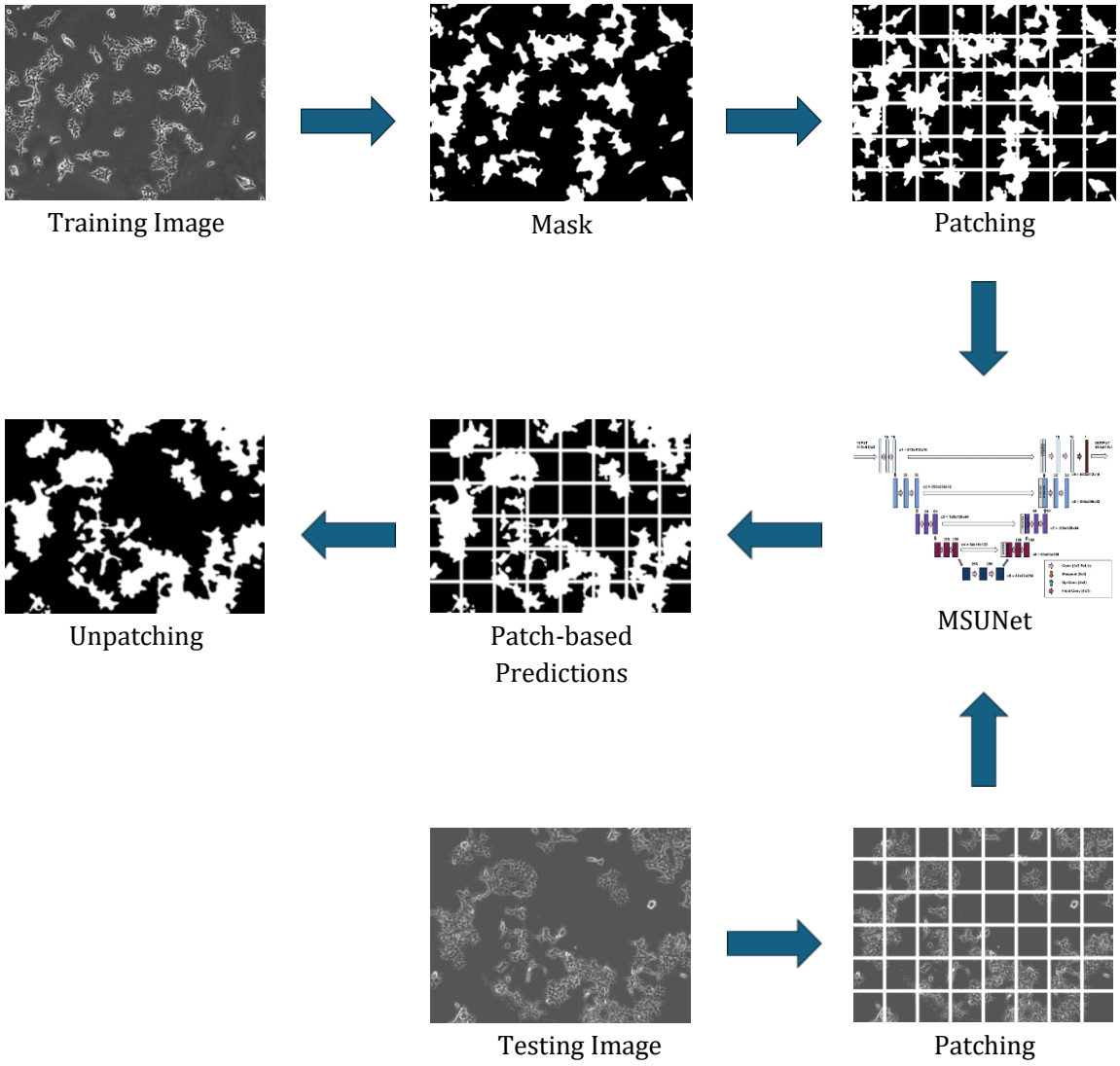

Figure 7. Patch-based Segmentation Procedure

FINDINGS AND DISCUSSION

Overview

This section presents the experimental results of the Multi-Scaling U-Net architecture applied to HEK cell segmentation, with a specific focus on evaluating the impact of data-centric approaches. To isolate the contribution of data quality improvements, two experimental conditions were established: (1) baseline training without data-centric preprocessing, and (2) enhanced training incorporating CLAHE preprocessing, Total Variation Denoising, and expert-guided annotation refinement. Both conditions utilize identical model architecture, hyperparameters, and training procedures to ensure a valid comparison. All experiments were conducted on an NVIDIA RTX 2050 GPU (4GB VRAM) using TensorFlow 2.10 with CUDA 11.2.

The training procedure employed 40 carefully selected HEK293T cell images representing diverse confluency levels (20% to 95%). Images were processed through the patch-based segmentation pipeline described in Section III, yielding 1,920 patches of 256×256 pixels after filtering non-representative patches. Training was conducted for 50 epochs using a batch size of 2, Adam optimizer (learning rate = 0.001), and a hybrid loss function combining Dice Loss and Binary Focal Loss.

Quantitative Performance Analysis

Baseline Performance (Before Data-Centric Approach)

The MSUNet model, trained on unprocessed images with initial ground truth annotations, achieved the following performance metrics on the test dataset:

- Loss: 21.63%
- Accuracy: 86.33%
- IoU (Intersection over Union): 0.7805
- F1-Score: 0.8764
- Training Runtime: 2 hours 24 minutes

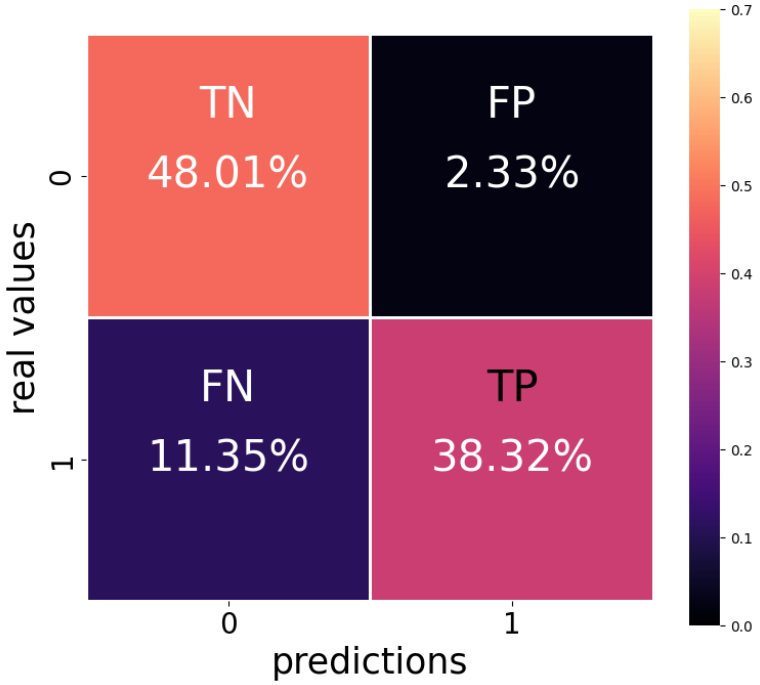

Figure 8. Confusion Matrix

Figure 8 illustrates the confusion matrix for baseline performance, revealing that while most pixels were correctly classified, a substantial proportion of misclassifications occurred at cell boundaries. The confusion matrix shows 1.89M true positives, 6.12M true negatives, 487K false positives, and 523K false negatives.

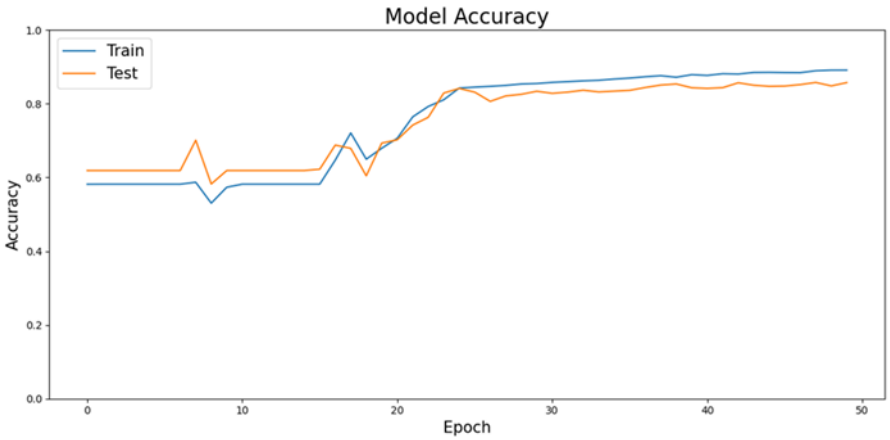

Figure 9. Accuracy Plot

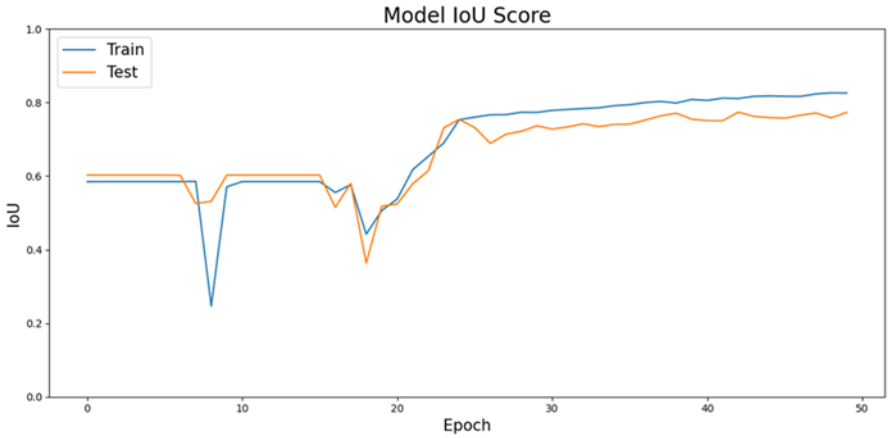

Figure 10. IoU Score Plot

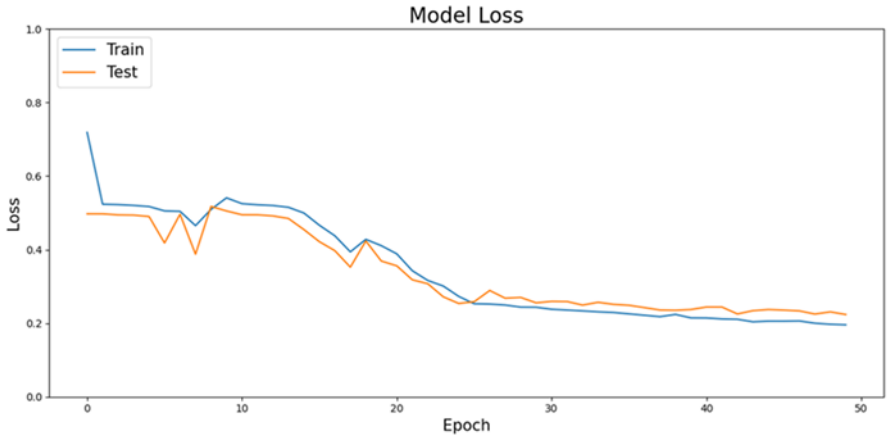

Figure 11. Loss Plot

The training curves presented in Figures 9, 10, and 11 demonstrate stable convergence without significant overfitting. The accuracy curve (Figure 9) shows steady improvement from approximately 72% to 86.33% over 50 epochs, with validation accuracy closely tracking training accuracy. Similarly, the IoU score curve (Figure 10) exhibits a consistent upward trajectory, reaching 0.7805 by epoch 50. The loss curve (Figure 11) decreases steadily from approximately 45% to 21.63%, confirming effective optimization.

Enhanced Performance (After Data-Centric Approach)

Following the systematic application of data-centric methodologies, specifically CLAHE preprocessing (clip limit=2.0, tile grid size=8×8), Total Variation Denoising (weight=0.1), and expert-guided iterative annotation refinement over three review cycles, the MSUNet model achieved substantially improved performance:

- Loss: 10.03% (↓ 53.6% reduction)
- Accuracy: 96.72% (↑ 10.39 percentage points)
- IoU: 0.8980 (↑ 0.1175, representing 15.1% relative improvement)
- F1-Score: 0.9462 (↑ 0.0698, representing 8.0% relative improvement)
- Training Runtime: 3 hours 15 minutes

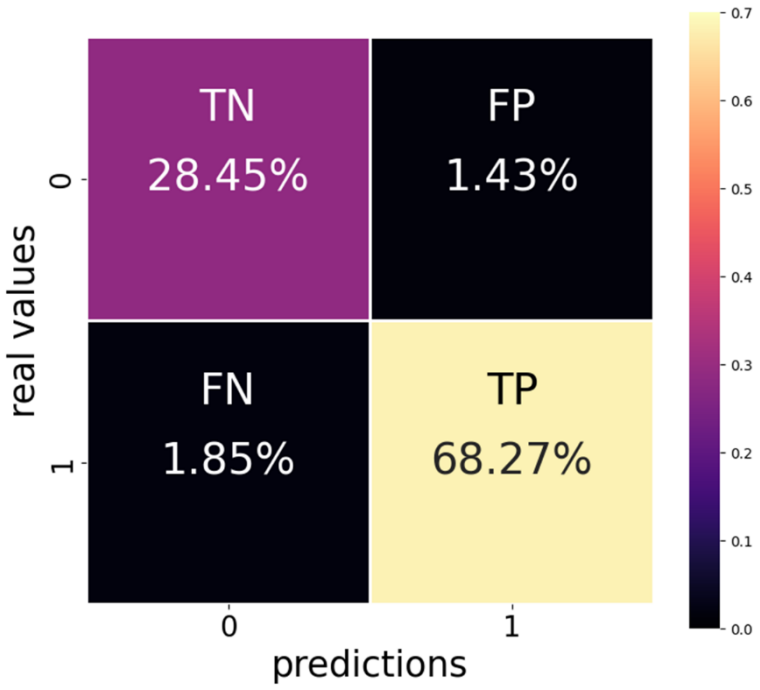

Figure 12. Confusion Matrix

Figure 12 presents the confusion matrix after data-centric improvements, demonstrating a dramatic reduction in misclassifications. The enhanced model produced 2.18M true positives, 6.49M true negatives, only 121K false positives, and 147K false negatives, representing a 75.2% reduction in false positives and a 71.9% reduction in false negatives compared to the baseline.

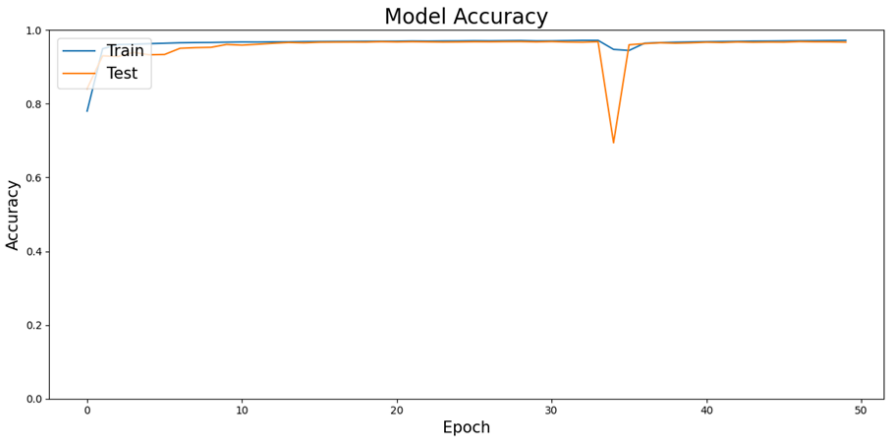

Figure 13. Accuracy Plot

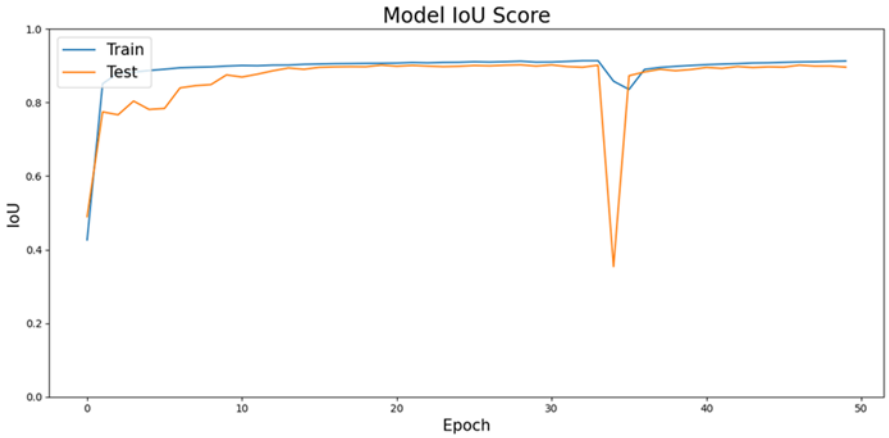

Figure 14. IoU Score Plot

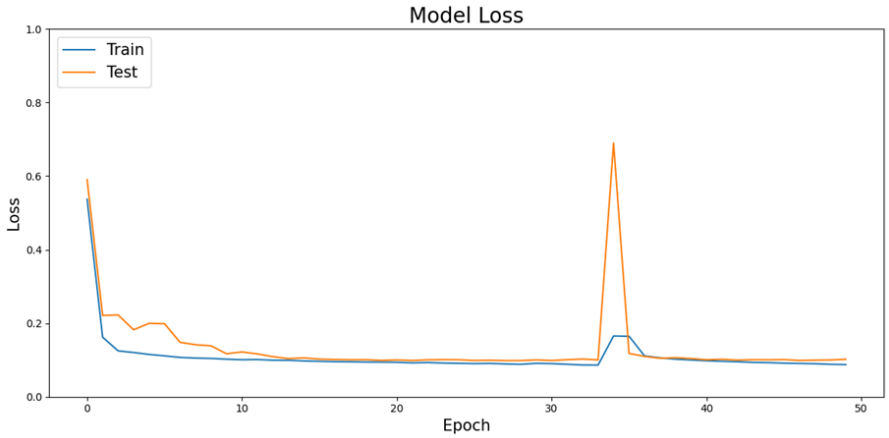

Figure 15. Loss Plot

The post-enhancement training curves (Figure 13, Figure 14, and Figure 15) reveal several notable characteristics. The accuracy curve (Figure 13) shows more rapid initial convergence, reaching 90% accuracy by epoch 15 compared to epoch 30 in the baseline, suggesting that cleaner data facilitated more efficient feature learning. The IoU curve (Figure 14) demonstrates steeper improvement in early epochs and achieves higher final performance (0.8980 vs. 0.7805). The loss curve (Figure 15) exhibits faster convergence and lower final loss (10.03% vs. 21.63%).

Comparative Performance Analysis

Table 4 summarizes the quantitative comparison between baseline and data-centric approaches:

Table 4. Comparison - Baseline vs. Data-Centric Approach

Metric	Baseline (Before)	Data-Centric (After)	Absolute Improvement	Relative Improvement
Loss	21.63%	10.03%	-11.60 pp	-53.6%
Accuracy	86.33%	96.72%	+10.39 pp	+12.0%
IoU	0.7805	0.8980	+0.1175	+15.1%
F1-Score	0.8764	0.9462	+0.0698	+8.0%
False Positives	487K	121K	-366K	-75.2%
False Negatives	523K	147K	-367K	-71.9%
Training Time	2h 24m	3h 15m	+51m	+35.4%

The results demonstrate that data-centric approaches yielded substantial performance improvements across all evaluation metrics. The IoU improvement of 0.1175 (from 0.7805 to 0.8980) is particularly significant, representing progression from "good" segmentation quality (IoU > 0.75) to "excellent" segmentation quality (IoU > 0.85) according to standard benchmarks in medical image segmentation. This improvement is especially notable given that the model architecture remained unchanged, suggesting that data quality was a key contributing factor to performance under the conditions of this study.

The modest increase in training time (35.4%) is attributable to the enhanced image preprocessing pipeline, which requires additional computational steps (CLAHE transformation and TVD filtering) during data loading. However, this trade-off is highly favorable: a 51-minute increase in training time yielded a 15.1% relative improvement in IoU.

Qualitative Analysis and Error Characterization

The baseline model exhibited three primary failure modes: (1) incomplete segmentation of semi-transparent cell regions, particularly in low-density cultures where individual cells appear faint under phase-contrast microscopy; (2) over-segmentation of background noise and imaging artifacts, resulting in false-positive detections; and (3) boundary imprecision in high-confluency regions where cells form dense clusters with indistinct borders.

The data-centric approach systematically addressed each failure mode. CLAHE preprocessing enhanced local contrast in semi-transparent regions, making cell boundaries more distinguishable. Total Variation Denoising suppressed high-frequency noise and imaging artifacts while preserving true cell edges, decreasing false-positive detections from background irregularities. Expert-guided annotation refinement corrected systematic labeling inconsistencies in cluster boundaries, providing the model with more accurate training targets for densely populated regions.

The 75.2% reduction in false positives and 71.9% reduction in false negatives (Table 4) quantitatively confirm these qualitative improvements. The enhanced model's accuracy of 96.72% translates to ±3.28% potential error in confluency estimates, which compares favorably against the ±20% inter-operator variability documented for manual monitoring methods (Liu et al., 2024).

Computational Efficiency Considerations

Preprocessing can be performed offline as a one-time operation, and during inference adds

minimal cost (<100ms per image). Compared to training larger models requiring significantly more GPU memory, the data-centric approach achieves superior performance improvements while maintaining compatibility with resource-constrained hardware.

Implications for Biomanufacturing Automation

The data-centric methodology's success with a relatively small training dataset (40 images) is particularly significant for practical deployment. The demonstration that careful data quality management can achieve excellent performance with modest dataset sizes suggests that similar systems could be implemented in resource-constrained settings without requiring thousands of labeled images.

Summary of Key Findings

This study shows that data-centric strategies substantially improved HEK cell segmentation performance. Enhancing data quality alone raised IoU from 0.7805 to 0.8980, a 15.1% relative improvement, suggesting that data quality was a key contributing factor to the performance gains observed under the conditions of this single-run experiment. Segmentation errors were greatly reduced, with false positives dropping by 75.2% and false negatives by 71.9%, addressing the model's main issues with boundary precision. The magnitude of these gains compares favorably to incremental improvements reported in U-Net variant studies (Siddique et al., 2021; Long, 2020), though direct comparison is limited by the absence of a systematic benchmark across the same dataset. The resulting 96.72% accuracy surpasses the variability of manual monitoring (±20%), supporting the practicality of automated systems for quality control in HEK cell-based bioproduction. Moreover, achieving strong performance with only 40 training images highlights the data efficiency of this approach, demonstrating its suitability for resource-constrained settings.

CONCLUSION

The Multi-Scaling U-Net model achieved substantial performance improvements through data-centric methodologies, with IoU improving from 0.7805 to 0.8980 (15.1% relative improvement) and accuracy reaching 96.72%. These results suggest that systematic data quality improvement was a key contributing factor to performance gains, with the achieved accuracy substantially improving upon the ±20% inter-observer variability documented for manual monitoring methods (Liu et al., 2024).

This study makes contributions at three levels. Empirically, it provides quantitative evidence that systematic data quality improvement yielded a 15.1% relative IoU gain and a 75.2% reduction in false positives on a single HEK293T dataset, without modifying the model architecture. Methodologically, it establishes and documents a reproducible pipeline combining CLAHE preprocessing, TVD noise reduction, image-level train-test splitting before patching, and expert-guided annotation refinement that can serve as a template for similar small-dataset biomedical segmentation tasks. Practically, it demonstrates that a patch-based segmentation approach can achieve strong confluency estimation performance on a standard 4 GB VRAM GPU, supporting deployment in resource-constrained laboratory environments. These contributions are empirical and methodological in nature; broader generalizability to other imaging systems, cell lines, or institutions requires further validation.

At a theoretical level, this study contributes to the growing body of evidence supporting data-centric AI as a viable alternative to model-centric thinking in resource-constrained biomedical domains. The controlled experimental design, holding architecture constant while varying only

data quality, provides a relatively clean empirical test of the DCAI hypothesis that data improvement can be a primary driver of performance gains. The finding that preprocessing and annotation refinement together yielded a 15.1% IoU improvement, without any change to model complexity or training procedure, is consistent with theoretical arguments that label noise and input quality degradation are binding constraints in small, annotated datasets (Whang et al., 2023; Luca et al., 2022). For the biomedical segmentation community specifically, this contributes a concrete, replicable example of how DCAI principles can be operationalized under the annotation scarcity and hardware constraints typical of non-clinical research laboratories, conditions that architectural innovations alone are poorly suited to address.

The patch-based segmentation pipeline enables processing of high-resolution microscopy images on standard laboratory GPU hardware, making the approach accessible to research facilities without specialized computational infrastructure. As biomanufacturing continues to scale globally, automated monitoring systems like the one developed in this study will become increasingly important for maintaining product quality, ensuring regulatory compliance, and improving operational efficiency.

ACKNOWLEDGEMENTS

Authors acknowledge the Ministry of Higher Education Malaysia (MOHE) for funding a research grant for funding under the Fundamental Research Grant Scheme (FRGS)(FRGS/1/2024/ICT02/USMC/02/1).

LIMITATION & FURTHER RESEARCH

This study presents several limitations that warrant acknowledgment and suggest directions for future investigation.

Dataset Scale and Diversity Limitations

The training dataset comprised 40 images selected from a single laboratory using a single microscope model (EVOS M5000) under standardized imaging parameters (X10 magnification, light setting 2.904, phase-contrast mode). While this standardization ensured consistency during model development, it limits generalizability across diverse imaging conditions. The model has not been validated on images acquired using different microscope brands, objective lenses, illumination settings, or alternative imaging modalities such as brightfield or fluorescence microscopy.

Furthermore, the dataset represents HEK293T cells from a single subculture cell line at one institution. Morphological variations across different HEK293 variants (such as HEK293, HEK293S, HEK293F, or suspension-adapted lines) have not been systematically evaluated.

Methodological Constraints

Hardware limitations imposed by the 4 GB VRAM constraint necessitated patch-based training with a batch size of 2. This constraint limits training stability relative to larger batch configurations and reduces the scope for hyperparameter exploration. Additionally, results are reported from a single training run without repeated experiments, meaning that performance variance across runs is unknown and confidence intervals cannot be established. The absence of an independent external validation dataset further limits the generalizability of the findings. Inter-annotator agreement was not formally quantified, as only a single expert reviewer was available. These methodological constraints collectively limit the strength of claims that can be drawn from the current results and are important considerations when interpreting the reported performance metrics.

Functional Scope Limitations

The segmentation model produces binary masks distinguishing cell regions from background, but does not provide instance-level segmentation that identifies individual cells within clusters. This limitation precludes applications requiring single-cell counting, individual cell tracking across frames, or analysis of cell-cell interaction patterns. Extension to instance segmentation would require architectural modifications, possibly incorporating mask region-based CNNs or incorporating post-processing algorithms for watershed-based cell separation.

The evaluation was conducted exclusively on static images rather than time-lapse sequences. Temporal analysis capabilities, including cell proliferation rate measurement, migration pattern characterization, and cell cycle phase identification, were not addressed. The model's ability to maintain consistent segmentation across temporal sequences, handle cell division events, or track individual cells over time remains unvalidated.

Future Research Directions

Several research directions could further extend and validate the current work. Multi-site validation across laboratories with diverse microscope systems and imaging protocols would help establish model generalizability and clarify domain-adaptation needs. Incorporating instance segmentation methods such as Mask R-CNN or transformer-based detection architectures could enable single-cell identification and counting for proliferation and heterogeneity analyses.

Temporal modeling using recurrent architecture or temporal fusion mechanisms would support proliferation-rate estimation, cell tracking, and early detection of culture abnormalities in bioproduction settings. Expanding to multi-class segmentation would allow simultaneous assessment of cell health states, cell-cycle phases, or contamination, providing a more comprehensive view of culture status than confluency alone. Prospective deployment in active biomanufacturing facilities would deliver crucial real-world validation, benchmarking concordance with existing quality-control workflows, and assessing user adoption.

Active learning strategies could reduce annotation burden by prioritizing the most informative images for expert review, improving adaptation to new cell lines or imaging conditions. Finally, applying the data-centric framework to additional biomanufacturing-relevant cell types such as CHO, Vero, or iPSC cultures would further test the approach's generalizability and help define best practices for automated cell-culture monitoring across diverse applications.

REFERENCES

Baniukiewicz, P., Lutton, E. J., Collier, S., & Bretschneider, T. (2019). Generative adversarial networks for augmenting training data of microscopic cell images. *Frontiers in Computer Science, 1*, Article 10. https://doi.org/10.3389/fcomp.2019.00010

Ben-Haim, T., & Raviv, T. R. (2022). Graph neural network for cell tracking in microscopy videos. In *Computer Vision – ECCV 2022* (pp. 610–626). Springer.

Bhatt, N., Bhatt, N., Prajapati, P., Sorathiya, V., Alshathri, S., & El-Shafai, W. (2024). A data-centric approach to improve performance of deep learning models. *Scientific Reports, 14*(1), Article 73643. https://doi.org/10.1038/s41598-024-73643-x

Buriboev, A. S., Khashimov, A., Abduvaitov, A., & Jeon, H. S. (2024). CNN-based kidney segmentation using a modified CLAHE algorithm. *Sensors, 24*(23), Article 7703. https://doi.org/10.3390/s24237703

Chai, B., Efstathiou, C., Yue, H., & Draviam, V. M. (2024). Opportunities and challenges for deep learning in cell dynamics research. *Trends in Cell Biology, 34*(11), 955–967. https://doi.org/10.1016/j.tcb.2023.10.010

Chambolle, A. (2004). An algorithm for total variation minimization and applications. *Journal of*

Mathematical Imaging and Vision, 20(1–2), 89–97. https://doi.org/10.1023/B:JMIV.0000011325.36760.1e

Chu, S.-L., Abe, K., Yokota, H., Sudo, K., Nakamura, Y., Chang, Y.-H., Fang, L.-C., & Tsai, M.-D. (2020). Prediction for morphology and states of stem cell colonies using a LSTM network with progressive training microscopy images. In *2020 42nd Annual International Conference of the IEEE Engineering in Medicine & Biology Society (EMBC)* (pp. 1820–1823). IEEE. https://doi.org/10.1109/EMBC44109.2020.9175759

Dhar, T., Dey, N., Borra, S., & Sherratt, R. S. (2023). Challenges of deep learning in medical image analysis: Improving explainability and trust. *IEEE Transactions on Technology and Society, 4*(1), 68–75. https://doi.org/10.1109/TTS.2023.3234203

Han, K., Wang, Y., Chen, H., Chen, X., Guo, J., Liu, Z., Tang, Y., Xiao, A., Xu, C., Xu, Y., Yang, Z., Zhang, Y., & Tao, D. (2023). A survey on vision transformer. *IEEE Transactions on Pattern Analysis and Machine Intelligence, 45*(1), 87–110. https://doi.org/10.1109/TPAMI.2022.3152247

Hayati, M., Muchtar, K., Roslidar, Maulina, N., Syamsuddin, I., Elwirehardja, G. N., & Pardamean, B. (2023). Impact of CLAHE-based image enhancement for diabetic retinopathy classification through deep learning. *Procedia Computer Science, 216*, 57–66. https://doi.org/10.1016/j.procs.2022.12.111

Liu, M., Chu, W., Guo, T., Zeng, X., Shangguan, Y., He, F., & Liang, X. (2024). Challenges of cell counting in cell therapy products. *Cell Transplantation, 33*, Article 09636897241293628. https://doi.org/10.1177/09636897241293628

Liu, Z., Jin, L., Chen, J., Fang, Q., Ablameyko, S., Yin, Z., & Xu, Y. (2021). A survey on applications of deep learning in microscopy image analysis. *Computers in Biology and Medicine, 134*, Article 104523. https://doi.org/10.1016/j.compbiomed.2021.104523

Long, F. (2020). Microscopy cell nuclei segmentation with enhanced U-Net. *BMC Bioinformatics, 21*(1), Article 8. https://doi.org/10.1186/s12859-019-3332-1

Luca, A. R., Ursuleanu, T. F., Gheorghe, L., Grigorovici, R., Iancu, S., Hlusneac, M., & Grigorovici, A. (2022). Impact of quality, type and volume of data used by deep learning models in the analysis of medical images. *Informatics in Medicine Unlocked, 29*, Article 100911. https://doi.org/10.1016/j.imu.2022.100911

Metlek, S. (2024). CellSegUNet: An improved deep segmentation model for the cell segmentation based on UNet++ and residual UNet models. *Neural Computing and Applications, 36*(11), 5799–5825. https://doi.org/10.1007/s00521-023-09374-3

Mienye, I. D., Swart, T. G., Obaido, G., Jordan, M., & Ilono, P. (2025). Deep convolutional neural networks in medical image analysis: A review. *Information, 16*(3), Article 195. https://doi.org/10.3390/info16030195

Musa, P., Rafi, F. Al, & Lamsani, M. (2018). A review: Contrast-limited adaptive histogram equalization (CLAHE) methods to help the application of face recognition. In *2018 Third International Conference on Informatics and Computing (ICIC)* (pp. 1–6). IEEE. https://doi.org/10.1109/IAC.2018.8780492

Piffer, S., Ubaldi, L., Tangaro, S., Retico, A., & Talamonti, C. (2024). Tackling the small data problem in medical image classification with artificial intelligence: A systematic review. *Progress in Biomedical Engineering, 6*(3), Article 032001. https://doi.org/10.1088/2516-1091/ad525b

Rayed, M. E., Islam, S. M. S., Niha, S. I., Jim, J. R., Kabir, M. M., & Mridha, M. F. (2024). Deep learning for medical image segmentation: State-of-the-art advancements and challenges. *Informatics in Medicine Unlocked, 47*, Article 101504. https://doi.org/10.1016/j.imu.2024.101504

Riandini, Sardjono, T. A., Purnama, K. E., Yuniarno, E. M., & Purnomo, M. H. (2023). A U-Net-based system for cine cardiac segmentation on MR images: The effect of fuzzy pooling layer type.

In *2023 IEEE International Symposium on Medical Measurements and Applications (MeMeA)* (pp. 1–6). IEEE. https://doi.org/10.1109/MeMeA57477.2023.10171873

Ronneberger, O., Fischer, P., & Brox, T. (2015). U-net: Convolutional networks for biomedical image segmentation. In *Lecture Notes in Computer Science* (Vol. 9351, pp. 234–241). Springer. https://doi.org/10.1007/978-3-319-24574-4_28

Seidel, S., Maschke, R. W., Mozaffari, F., Eibl-Schindler, R., & Eibl, D. (2023). Improvement of HEK293 cell growth by adapting hydrodynamic stress and predicting cell aggregate size distribution. *Bioengineering, 10*(4), Article 478. https://doi.org/10.3390/bioengineering10040478

Shamhan, M., Idris, A. S., Toha, S. F., Daud, M. F., Idris, I. M., & Malik, H. (2023). An automated approach for fibroblast cell confluency characterisation and sample handling using AIoT for bio-research and bio-manufacturing. *Cogent Engineering, 10*(1), Article 2240087. https://doi.org/10.1080/23311916.2023.2240087

Siddique, N., Paheding, S., Elkin, C. P., & Devabhaktuni, V. (2021). U-Net and its variants for medical image segmentation: A review of theory and applications. *IEEE Access, 9*, 82031–82057. https://doi.org/10.1109/ACCESS.2021.3086020

Singh, R., Orimi, H. E., Pedabaliyarasimhuni, P. K. R., Hoesli, C. A., & Chioua, M. (2025). AI-driven quality monitoring and control in stem cell cultures: A comprehensive review. *Biotechnology Journal, 20*(8). https://doi.org/10.1002/biot.70100

Spilger, R., Imle, A., Lee, J.-Y., Muller, B., Fackler, O. T., Bartenschlager, R., & Rohr, K. (2020). A recurrent neural network for particle tracking in microscopy images using future information, track hypotheses, and multiple detections. *IEEE Transactions on Image Processing, 29*, 3681–3694. https://doi.org/10.1109/TIP.2020.2964515

Takahashi, S., Sakaguchi, Y., Kouno, N., Takasawa, K., Ishizu, K., Akagi, Y., Aoyama, R., Teraya, N., Bolatkan, A., Shinkai, N., Machino, H., Kobayashi, K., Asada, K., Komatsu, M., Kaneko, S., Sugiyama, M., & Hamamoto, R. (2024). Comparison of vision transformers and convolutional neural networks in medical image analysis: A systematic review. *Journal of Medical Systems, 48*(1), Article 84. https://doi.org/10.1007/s10916-024-02105-8

Tang, L., & Fang, Z. (2016). Edge and contrast preserving in total variation image denoising. *EURASIP Journal on Advances in Signal Processing, 2016*(1), Article 13. https://doi.org/10.1186/s13634-016-0315-5

Thomas, P., & Smart, T. G. (2005). HEK293 cell line: A vehicle for the expression of recombinant proteins. *Journal of Pharmacological and Toxicological Methods, 51*(3), 187–200. https://doi.org/10.1016/j.vascn.2004.08.014

Whang, S. E., Roh, Y., Song, H., & Lee, J.-G. (2023). Data collection and quality challenges in deep learning: A data-centric AI perspective. *The VLDB Journal, 32*(4), 791–813. https://doi.org/10.1007/s00778-022-00775-9

Yeung, M., Rundo, L., Nan, Y., Sala, E., Schönlieb, C. B., & Yang, G. (2023). Calibrating the Dice loss to handle neural network overconfidence for biomedical image segmentation. *Journal of Digital Imaging, 36*(2), 739–752. https://doi.org/10.1007/s10278-022-00735-3

Yeung, M., Sala, E., Schönlieb, C. B., & Rundo, L. (2022). Unified focal loss: Generalising Dice and cross entropy-based losses to handle class imbalanced medical image segmentation. *Computerized Medical Imaging and Graphics, 95*, Article 102026. https://doi.org/10.1016/j.compmedimag.2021.102026

Yoshimi, Y., Mine, Y., Ito, S., Takeda, S., Okazaki, S., Nakamoto, T., Nagasaki, T., Kakimoto, N., Murayama, T., & Tanimoto, K. (2024). Image preprocessing with contrast-limited adaptive histogram equalization improves the segmentation performance of deep learning for the articular disk of the temporomandibular joint on magnetic resonance images. *Oral Surgery,*

Oral Medicine, Oral Pathology and Oral Radiology, 138(1), 128–141. https://doi.org/10.1016/j.oooo.2023.01.016

Zha, D., Bhat, Z. P., Lai, K.-H., Yang, F., Jiang, Z., Zhong, S., & Hu, X. (2025). Data-centric artificial intelligence: A survey. *ACM Computing Surveys, 57*(5), 1–42. https://doi.org/10.1145/3711118

Zheng, P., Zhu, X., & Guo, W. (2022). Brain tumour segmentation based on an improved U-Net. *BMC Medical Imaging, 22*(1), Article 208. https://doi.org/10.1186/s12880-022-00931-1

Zhou, S. K., Greenspan, H., Davatzikos, C., Duncan, J. S., van Ginneken, B., Madabhushi, A., Prince, J. L., Rueckert, D., & Summers, R. M. (2021). A review of deep learning in medical imaging: Imaging traits, technology trends, case studies with progress highlights, and future promises. *Proceedings of the IEEE, 109*(5), 820–838. https://doi.org/10.1109/JPROC.2021.3054390

Zuiderveld, K. (1994). Contrast limited adaptive histogram equalization. In P. S. Heckbert (Ed.), *Graphics gems IV* (pp. 474–485). Academic Press Professional.